



Supporting Online Material for

Undulatory Swimming in Sand: Subsurface Locomotion of the Sandfish Lizard

Ryan D. Maladen, Yang Ding, Chen Li, Daniel I. Goldman*

*To whom correspondence should be addressed. E-mail: daniel.goldman@physics.gatech.edu

Published 17 July 2009, *Science* **325**, 314 (2009)

DOI: 10.1126/science.1172490

This PDF file includes:

Materials and Methods

Figs. S1 to S3

Table S1

References

Other Supporting Online Material for this manuscript includes the following:

(available at www.sciencemag.org/cgi/content/full/325/5938/314/DC1)

Movies S1 to S3

Corrections: Equations S4, S7, and S12 were missing square root symbols; this was an error introduced in proofs and they have been restored.

Equation S11 is now correctly labeled as Equation S11.

The section “Analytic Solution of Small Amplitude Resistive Force Model” has been more accurately retitled “Approximate Analytic Solution of the Resistive Force Model.”

Undulatory swimming in sand: subsurface locomotion of the sandfish lizard - Supplement

Ryan D. Maladen¹, Yang Ding², Chen Li² and Daniel I. Goldman,^{2,1*}

¹Interdisciplinary Bioengineering Program

²School of Physics, Georgia Institute of Technology,
Atlanta, GA 30332, USA

*E-mail: daniel.goldman@physics.gatech.edu

Materials and Methods

Sandfish X-ray Experiments

Sandfish lizards (*Scincus scincus*) were obtained from a commercial supplier (LLL Reptile, CA, USA), housed in a dedicated animal care facility, and kept in a 12 hour day/night light cycle. The average snout vent length (SVL), which we denote as body-length L in the manuscript and which is $\approx 75\%$ of the snout-tip to tail-tip length, was 8.3 ± 3.3 cm. The average mass was 16.2 ± 4 grams. High speed (250 fps) x-ray and visible light video of the sandfish were taken as they moved on and within a 10 cm deep layer of granular material (0.27 ± 0.04 mm diameter spherical glass beads, density $\rho \approx 2.4$ g/cm³) held in a container (21.5 cm \times 18 cm). The granular material was prepared in two volume fractions ($\phi = 0.58$ and $\phi = 0.62$), loose and close packings for dry grains. The material state was set using an air fluidized bed, a counter flow of air to a collection of granular media. Below a critical flow rate (the onset of fluidization), grains are stationary; above it, the material is fluidized and grains flow. To generate loosely packed states ($\phi = 0.58$) the flow is increased to above the fluidization onset and then slowly decreased to zero. To generate closely packed states the air flow is repeatedly pulsed. Increasing the number of pulses increases ϕ ; typically we delivered over 200 pulses to achieve the closely packed state ($\phi = 0.62$).

The x-ray system (Radiological Imaging Systems, OEC 9000) energy was varied in the range of 85 – 100 kV at 20 mA. After the x-ray beam was turned on, a gate to a holding pen was rapidly raised to release the animal onto the surface of the granular media. A thin above-ground plexiglas barrier (visible in Movies S1 and S2) forced the animal into the dive at the

same location in the bed. The animal consistently took a few steps and then dove into the material. The sandfish appears dark in the above ground x-ray images since the radiation must travel through the sand and the animal, while below ground it appears lighter since sand has been displaced horizontally by the body of the organism. Experiments were conducted between 30 and 35 °C.

The x-ray (Movies S2 and S3) and visible light (Movie S1) videos were synchronized to determine when the sandfish was moving subsurface. The temporal frequency and forward velocity of the animal were measured from this section of video. Displacement was calibrated using a grid. X-ray visible natural body markers (the snout and lungs) as well as the silhouette of the animal were used to estimate the mid-line of the animal and track it using MATLAB. The digitized undulation profiles of the animal were fit with the equation of a sinusoidal traveling wave to obtain the spatial and temporal characteristics of the animal. We collected representative runs with opaque markers bonded to the body midline and limbs of the sandfish to verify the lack of limb use subsurface (Movie S3). The total mass of the markers was 0.04 g, much less than the 16 g animals, The inter-limb distance measure allowed us to determine the nature of limb use subsurface and contrast it with the diagonal gait used in surface locomotion. The visible light video was used to determine the sandfish burial time.

Our model (explained later) suggests (Fig. S3) that the variability in the animal (the spread in velocity for a given frequency) is a result of the sensitivity of the swimming speed to small changes (within experimental variation during a swim) in both the amplitude and the wavelength.

Resistive Force Theory for Granular Media

We developed our Resistive Force Theory for sandfish locomotion in granular media based on work by Gray & Hancock (SI) for non-inertial low Re swimmers. The animal is modeled as a flexible cylinder with a sinusoidal traveling wave progressing from head to tail (Fig. 3A) such that:

$$y = A \sin \frac{2\pi}{\lambda}(x + v_w t), \quad (S1)$$

where y is the displacement away from the midline of a straight animal, A the amplitude, λ the wavelength, f the wave frequency, and $v_w = f\lambda$ the wave speed. For a given forward velocity v_x , other quantities characterizing the motion can be calculated:

$$\begin{aligned} v_y &= \frac{dy}{dt} = \frac{2A\pi v_w}{\lambda} \cos \frac{2\pi}{\lambda}(x + v_w t) \\ \tan \theta &= \frac{dy}{dx} = \frac{2A\pi}{\lambda} \cos \frac{2\pi}{\lambda}(x + v_w t) \\ \psi &= \arctan\left(\frac{v_y}{v_x}\right) - \theta, \end{aligned} \quad (S2)$$

where θ is the angle of the axis of an infinitesimal cylindrical element with respect to the forward direction and ψ the angle between the axis of the element and its instantaneous velocity.

We assume that the forces F_N and F_L (see Fig. 3A for the force diagram, and text and **Rod Drag Empirical Fitting Function** section for discussion of the force model) on an infinitesimal element of the animal are proportional to the area of the longitudinal cross section $\delta A = 2r\delta s$ and are functions of ψ . The resultant force on the element in the forward direction (+ x -axis) is:

$$\delta F_x = (P_N \sin \theta - P_L \cos \theta)2r\delta s, \quad (\text{S3})$$

where P_N and P_L are the forces per cross section area normal and parallel to the axis of the element. Then the total force on the body F_{bx} in the direction of motion can be expressed as

$$F_{bx} = \int_0^\lambda (P_N \sin \theta - P_L \cos \theta) \sqrt{1 + \tan^2 \theta} 2r dx. \quad (\text{S4})$$

Although the angle of each element changes in time, since the integral is over one full wavelength the integral in Equation S4 is time invariant.

Equation S4 accounts for forces acting on the body but not the head. To account for the head we use two limits, a flat head that produces maximum drag and no head which produces no drag. For the flat head model (FH), we assume that the drag on the head F_h is the same as the drag on the flat end face of a rod in our experiment. This drag is decomposed into two orthogonal components F_N^T and F_L^T and its form is approximated by Equation S8, setting the length $l = 0$ and r as the average radius of the sandfish. The net force in the forward (+ x) direction on the head is:

$$F_{hx}(t) = F_N^T \sin \theta - F_L^T \cos \theta. \quad (\text{S5})$$

The drag force on the head is set to zero for the no head model (NH).

The time average of the force on the head (\bar{F}_{hx}) is equal to the spatial average:

$$\bar{F}_{hx} = \frac{1}{T} \int_0^T F_{hx} dt = \frac{1}{\lambda} \int_0^\lambda (F_N^T \sin \theta - F_L^T \cos \theta) dx. \quad (\text{S6})$$

Combining the head drag with the body force we obtain the total time averaged force on the sandfish:

$$\begin{aligned} \bar{F}_x = \int_0^\lambda [(P_N(\psi) \sin \theta - P_L(\psi) \cos \theta) \sqrt{1 + \tan^2 \theta} 2r \\ + (F_N^T \sin \theta - F_L^T \cos \theta) / \lambda] dx. \end{aligned} \quad (\text{S7})$$

At constant average velocity, \bar{F}_x is zero. The forward velocity v_x can then be found numerically if v_w , A , λ , $P_N(\psi)$ and $P_L(\psi)$ are known. Since the wave and body velocities in Equation S7 only appear as ratios (see Equation S2) and do not appear in expressions for P_N or P_L , a proportional relation between v_x and v_w is expected. We can thus solve for the wave efficiency $\eta = v_x/v_w$. Figure S3 shows that η increases rapidly with increasing A/λ for $A/\lambda \lesssim 0.3$ and increases slowly for $A/\lambda \gtrsim 0.3$.

Drag Experiments in Granular Media

To obtain expressions for the forces on the sandfish, we moved a stainless steel cylindrical cylinder representing a sandfish body element through granular media at constant velocity (10 cm/s) and measured the resulting normal and lateral forces for angles ψ between the element and its displacement direction ranging from 0° to 90° (Fig. 3 C and D, and Fig. S2 C). We used a fluidized bed (filled to a depth of 12 cm) to set the initial volume fraction (ϕ) of the media. We chose stainless steel because a previous study (S2) as well as our measurements have shown that sandfish skin and stainless steel have about the same friction coefficient with sand (~ 0.2). The diameter of the cylinder ($2r = 1.58$ cm) is similar to that of the sandfish body (1.75 cm). To avoid effects on the drag due to the finite size of the container, the cylinder is small compared to the size of the fluidized bed but large compared to the size of the grains. The cylinder is attached to a robotic arm (CRS Robotics) via a thin but stiff supporting rod which moves the structure at constant depth and velocity while a 6 d.o.f. force sensor (ATI industrial) mounted between the robotic arm and the supporting rod measures the net force generated during the drag motion (accurate to 0.06 N). The force on the supporting pole is also measured separately and subtracted to obtain the force on just the cylinder.

Previous studies show that drag in granular media is independent of speed (S3, S4) and increases proportionally to depth (S3). To test if this effect persisted in the regime relevant to the sandfish (0-40 cm/s), we dragged the cylinder perpendicular to velocity at 1, 5, 10, 20, and 30 cm/s (which covers the sandfish's range of speeds) at a fixed depth of 7.62 cm and found that over an order of magnitude change in speed, force only changed by 10% (Fig. S2 B); consequently we assumed force is independent of speed. We also dragged the cylinder oriented perpendicular to velocity at different depths (1.27, 2.54, 3.81, 5.08, 6.35, and 7.62 cm) at 10 cm/s and confirmed that as seen previously (S3) drag is proportional to depth (Fig. S2 A). Therefore, we measured drag force on the cylinder as a function of angle (for input into the Resistive Force Theory model) by dragging the cylinder at a fixed depth (7.62 cm) and a constant speed of 10 cm/s for different ϕ .

Before each trial, the initial state of the medium was set using a fluidized bed and the test rod rotated to the desired angle using the robotic arm. For each angle the rod was pushed into the material to a depth of 7.62 cm and, after a 2 second pause, was dragged for 15.24 cm through the medium and then extracted. Both the force and position of the rod were recorded at 140 Hz. The forces parallel (F_L) and perpendicular (F_N) to the surface of the rod were resolved by the force sensor and averaged over the steady state drag region (Fig. 3 B). Three trials were conducted for each ψ and ϕ .

Rod Drag Empirical Fitting Function

To characterize the relation between the measured values of normal and lateral drag force on the rod and its orientation ψ relative to the direction of motion we developed an empirical fitting function inspired by soil mechanics (S5). Because there is a drag induced normal force

perpendicular to the front half of the surface of the rod, there are two contributions to the resistive force in the horizontal plane of the motion. The first is the in-plane component of the normal force, characterized by C_S , and from the velocity independence of force (Fig. S2 B) we expect to be constant. The second is the in-plane component of the frictional force acting everywhere tangential to the surface of the rod characterized by C_F . We expect the planar normal force to be larger than the frictional force because the friction between the grains and the rod is less than unity. The total force has contributions from the sidewall of the cylinder and the flat ends. For a cylinder with length l and radius r , the total forces F_N^T and F_L^T can be written as:

$$\begin{aligned} F_N^T &= 2lr(C_S \sin \beta_0 + C_F \sin \psi) + \pi r^2 C_F \sin(\psi) \\ F_L^T &= 2lrC_F \cos \psi + \pi r^2 C_S \sin \beta'_0, \end{aligned} \quad (\text{S8})$$

where $\tan \beta_0 = \cot \gamma_0 \sin \psi$ and $\tan \beta'_0 = \cot \gamma_0 \sin(\pi/2 - \psi)$ and γ_0 is a parameter related to the internal slip angle in granular media (S5).

The total forces F_N^T and F_L^T are determined as the averages over the shaded region in Fig. 3B. The fits to the measurements of F_N^T and F_L^T determine the three parameters C_S , C_F and γ_0 . These parameters are given in Table S1 and are used in Equation 1 to approximate the forces on the body F_N and F_L as the forces on the sidewalls of the cylinder without contributions from the flat ends (subtracting terms proportional to the flat end area, πr^2).

Approximate Analytic Solution of the Resistive Force Model

To gain insight into how η depends on kinematic parameters and features of the force model, we develop an approximate analytic expression assuming small amplitude oscillations such that θ is small, and small slip (high η) such that we approximate $\arctan(v_y/v_x)$ as v_y/v_x . Using Equation S2, ψ can be approximated as

$$\begin{aligned} \psi &= \arctan\left(\frac{v_y}{v_x}\right) - \theta \\ \psi &\approx \frac{v_y}{v_x} - \theta \\ \psi &\approx \frac{1}{v_x} \frac{2A\pi v_w}{\lambda} \cos \frac{2\pi}{\lambda}(x + v_w t) - \frac{2A\pi}{\lambda} \cos \frac{2\pi}{\lambda}(x + v_w t), \end{aligned} \quad (\text{S9})$$

and since $\eta = v_x/v_w$,

$$\psi = \left(\frac{1}{\eta} - 1\right) \frac{2A\pi}{\lambda} \cos \frac{2\pi}{\lambda}(x + v_w t). \quad (\text{S10})$$

The equation above shows that ψ decreases as η increases and ψ oscillates along the body. For a sandfish swimming in a horizontal plane, the forces are only functions of ψ and the sum of thrust and drag forces on the body is found from Equation S4.

Assuming large η , we approximate P_N and P_L as the low ψ region of the curves in Fig. 3C and D. Thus the force per unit area is approximated as,

$$\begin{aligned} P_N &= C_N \psi \\ P_L &= C_L, \end{aligned} \tag{S11}$$

where C_N and C_L are constants characterizing the granular medium's drag.

Using these approximations, the integral becomes:

$$\begin{aligned} F_{bx} &= \int_0^\lambda (C_N \psi \sin \theta - C_L \cos \theta) \sqrt{1 + \tan^2 \theta} 2r dx \\ F_{bx} &= \int_0^\lambda \left\{ C_N \left(\frac{1}{\eta} - 1 \right) \frac{2A\pi}{\lambda} \cos \left[\frac{2\pi}{\lambda} (x + v_w t) \right] \sin \theta - C_L \cos \theta \right\} \sqrt{1 + \tan^2 \theta} 2r dx \\ F_{bx} &\approx \int_0^\lambda \left\{ C_N \left(\frac{1}{\eta} - 1 \right) \frac{2A\pi}{\lambda} \cos \left[\frac{2\pi}{\lambda} (x + v_w t) \right] \frac{2A\pi}{\lambda} \cos \left[\frac{2\pi}{\lambda} (x + v_w t) \right] - C_L \right\} 2r dx \\ F_{bx} &= \left[\frac{1}{2} C_N \left(\frac{1}{\eta} - 1 \right) \left(\frac{2A\pi}{\lambda} \right)^2 - C_L \right] 2r \lambda. \end{aligned} \tag{S12}$$

Note that $v_w t$ does not appear in the final form because the integral over a wavelength is independent of the initial phase. If we assume that for small θ the head drag is a constant F_{hx} , and we set the net force to zero:

$$F_{xnet} = \left[\frac{1}{2} C_N \left(\frac{1}{\eta} - 1 \right) \left(\frac{2A\pi}{\lambda} \right)^2 - C_L \right] 2r \lambda - F_{hx} = 0. \tag{S13}$$

The wave efficiency η can be found analytically. With $F_{hx} = 0$ the form of the solution is straightforward:

$$\eta = \frac{1}{1 + \frac{2C_L}{C_N} \left(\frac{\lambda}{2\pi A} \right)^2}. \tag{S14}$$

Estimating $C_N/C_L \approx 4$ and taking $A/\lambda \approx 0.2$ from the measured kinematics, Equation S14 gives $\eta = 0.76$. If the coefficient for head drag is estimated as C_N , then $\eta = 0.65$. The overestimate is likely due to the poor approximation of $\arctan(v_y/v_x) \approx v_y/v_x$, since for typical swimming speeds when v_y is maximal, $v_y/v_x \approx 2.5$ and thus $\arctan(v_y/v_x) \approx 1.2$.

Assumptions and Error Analysis

There are several assumptions in our model of sandfish swimming, including those in the RFT, in the estimates of F_N and F_L from the rod drag experiments, in the empirical fitting function, in the body shape, and in the form of the drag on the head. 1) The RFT assumes that the organism swims in a horizontal plane, while in reality it moves into the material in a plane inclined at

22° relative to the surface (*S6*). Since both drag and thrust are distributed over the body and are linear with depth (*S4*), we use the force on the central element as the average for the whole body. From x-ray data, the sandfish's head is ~ 3 cm and its central element about ~ 2 cm below the surface when the sandfish stops. Thus the force per area for the head is estimated to be 1.5 times larger than on the middle of the body. We assume $F_N(\psi)$ and $F_L(\psi)$ are the same as for horizontal drag. The projected force of gravity on the sandfish along the plane is neglected as it is small compared to the resistive force from the material (the ratio is estimated to be under 2%). We scaled the measured wavelength by $1/\cos(22^\circ) = 1.08$ to account for the projected wavelength on the horizontal plane of the x-ray images. 2) The forces used in the model are measured as the rod is dragged at constant velocity. In reality the velocity of each point on the body varies sinusoidally as the animal moves forward. 3) The diameter of the sandfish changes from head to tail, while a single diameter of 1.75 cm is used for the model. We approximated the sandfish as a single cylinder of fixed radius for simplicity of the model and calculation (i.e. time invariance of Equation S4). Since in the animal the radius shrinks near the head and tail, the surface of the body is not parallel to the spine of the sandfish. Our model predicts that the change in the diameter near the head (which results in a smaller ψ than in the uniform cylinder), causes decreased F_N and increased F_L . The taper of the tail results in larger ψ compared to the uniform cylinder which results in increased F_N and decreased F_L . We hypothesize that these effects result in a cancelation that makes the uniform cylinder a good approximation. 4) Since we did not have an estimate for the drag on the shovel shaped head of the sandfish, we computed η for two cases of head drag. We considered drag on the head zero (NH in Fig. 4A and S3) or that of a flat disk of radius comparable to the sandfish (FH). These predictions in conjunction with the model for body drag bound the experimentally measured η . With the model assumptions in place, the major contribution to the uncertainty in η comes from the experimentally measured run to run variation in the spatial parameters A and λ .

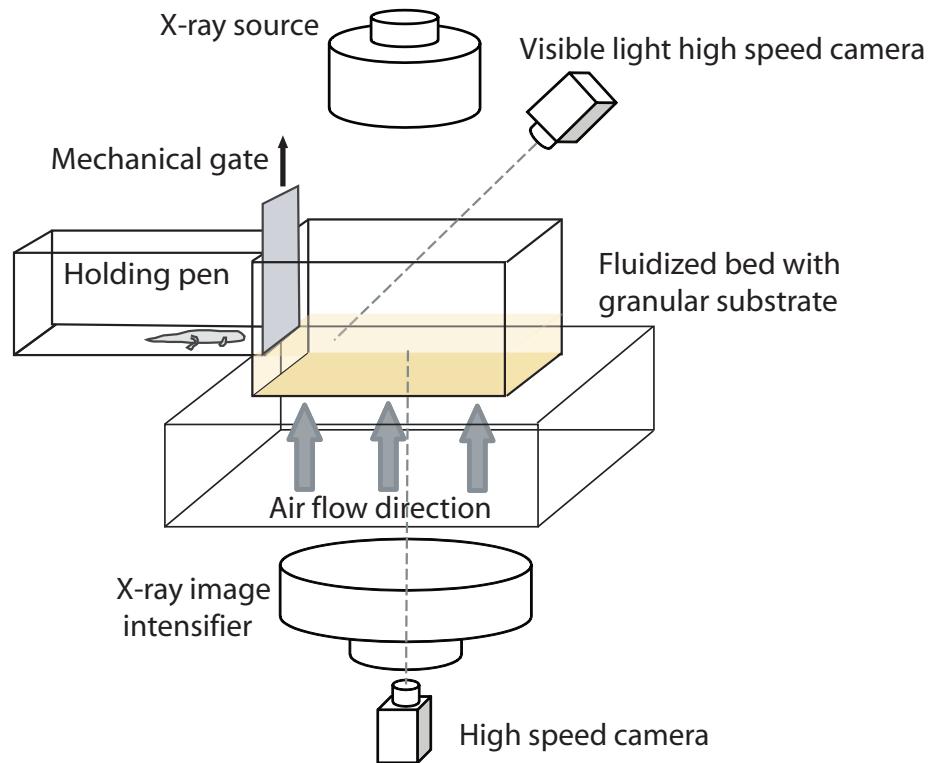


Figure S1: Experimental setup: a fluidized bed is placed between the source and image intensifier of a c-arm x-ray system. The initial state of the granular media (0.3 mm spherical glass beads) used to fill the fluidized bed is set using air pulses. Once the material is prepared the sandfish is released from the holding pen using a mechanical gate. Simultaneous x-ray and visible light video (250 fps) are recorded as the animal moves above and then below the surface. Drawings are not to scale.

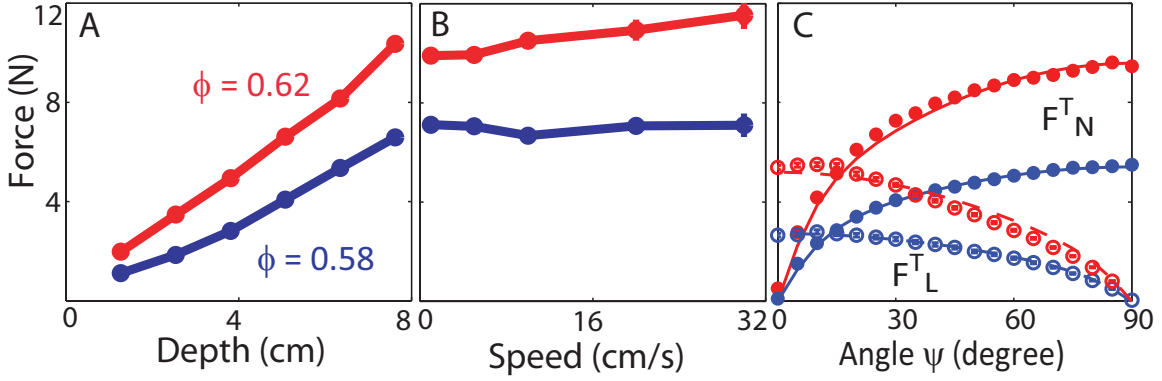


Figure S2: Force on a stainless steel cylinder as it is dragged at different depths, velocities, and angles through granular media of low and high ϕ . In (A) and (B) the cylinder is oriented perpendicular to the direction of motion. Average force vs. (A) depth and (B) speed for closely (red) and loosely (blue) packed preparations. (C) Average total forces (including sidewalls and end-faces) F_N^T (closed symbols) and F_L^T (open symbols) on the cylinder where the color of the symbols denote closely (red) and loosely (blue) packed preparations. Solid and dashed lines are model fits described by Equation S8. All forces are calculated by averaging instantaneous forces over steady state motion (e.g., see gray region in Fig. 3B); there is a 94% probability that the mean forces fall within the error bars (which are comparable to the symbol size).

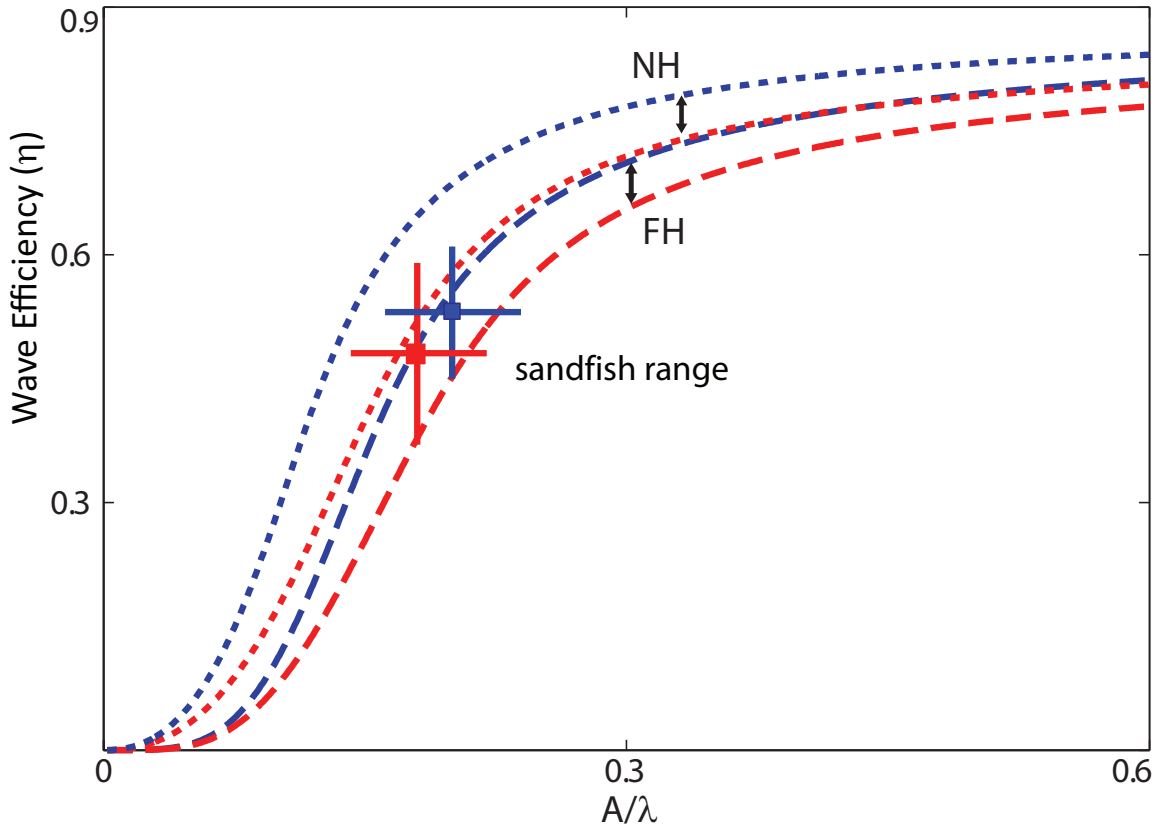


Figure S3: The wave efficiency predicted by the RFT model (numerical integration of the full model, Equation S7) is plotted against the spatial characteristic (A/λ) of the sinusoid. The blue and red curves correspond to predictions for LP and CP respectively. The red and blue squares with error bars show η measured from the kinematics of the sandfish in the x-ray experiments. Curves show model predictions using flat head (longer dash) and no head (shorter dash) limits.

Packing	ϕ	C_S ($\text{N/m}^2 \times 10^{-4}$)	C_F ($\text{N/m}^2 \times 10^{-4}$)	γ_0 (degree)
LP	0.58	0.51	0.28	13.84
CP	0.62	0.77	0.59	12.21

Table S1: The coefficients of the rod drag model: quantities related to the yield stress of the granular media (C_S), the flow resistance coefficient (C_F), and the internal slip angle of the granular media under gravity (γ_0).

Supplementary References

- S1. J. Gray, G. J. Hancock, *Journal of Experimental Biology* **32**, 802 (1955).
- S2. W. Baumgartner, et al., *Journal of Bionic Engineering* **4**, 1 (2007).
- S3. K. Wieghardt, *Annual Review of Fluid Mechanics* **7**, 89 (1975).
- S4. R. Albert, M. Pfeifer, A. Barabási, P. Schiffer, *Physical Review Letters* **82**, 205 (1999).
- S5. R. Nedderman, *Statics and kinematics of granular materials* (Cambridge University Press, 1992).
- S6. W. Baumgartner, et al., *PLoS ONE* **3**, e3309:1 (2008).